Anthony J MacKay Student Paper Contest

WINNER

The Anthony J. MacKay Student Paper Contest is organized each year by CRPA's Student Affairs Committee. The winner receives an all-expenses paid trip to the CRPA conference to present their paper. At the conference, the winner has an opportunity to meet professionals who work in the field of radiation science—hospitals, universities, the nuclear power industry, and all levels of government. The winning paper is also published in the CRPA *Bulletin*.

The contest is open to full- or part-time students at a Canadian university or college whose post-secondary studies are related to radiation sciences (nuclear medicine, medical physics, radiation therapy, etc.). The topic of the papers must be a radiation-related topic.

This year's winner was Steven Bartolac. His paper was co-authored by David Jaffray, his graduate supervisor.

Le concours de présentations étudiantes Anthony J. MacKay est organisé tous les ans par le comité de liaison avec les étudiants de l'ACRP. Le gagnant se mérite un voyage toutes dépenses payées au congrès de l'ACRP afin d'y présenter son article. Au congrès, le gagnant a l'occasion de rencontrer des professionnels qui travaillent dans le domaine de la science du rayonnement : hôpitaux, universités, industrie des centrales nucléaires et tous les niveaux gouvernementaux. La présentation du gagnant est également publiée dans les pages du Bulletin de l'ACRP.

Le concours s'adresse à tous les étudiants inscrits à temps plein ou partiel dans une université, un collège ou un CEGEP du Canada, dans un programme lié aux sciences du rayonnement (médecine nucléaire, physique médicale, radiothérapie, etc.). Enfin, le sujet des présentations doit être lié aux rayonnements.

Le gagnant de cette année est Steven Bartolac et son article a été corédigé par David Jaffray, son superviseur d'études.

Fluence Field Modulated CT

Potential for Dose and Noise Optimization in Thoracic Imaging Applications

Steven Bartolac (Department of Medical Biophysics, University of Toronto)
David Jaffray (Department of Radiation Oncology, University of Toronto)

Introduction

Recently, awareness regarding the potential risks of radiation dose due to computed tomography (CT) scans has been raised both in the general public, via reports in mainstream media, as well as among medical practitioners and physicists. A notable example of the former is the article "How Dangerous Are CT Scans," which appeared in Time magazine (Guthrie, 2008). The latter has been evidenced in North America most significantly through the widespread campaigns Image Gently and Image Wisely, which have the general mandate of providing education on how to limit unnecessary dose to pediatric and adult patients respectively.

The heightened concern regarding the radiation risks of CT has been largely stimulated by a number of reports and papers within the last five years (Brenner and Hall 2007; Hillman and Goldsmith 2010; Smith-Bindman 2010), which have indicated both that the number of CT procedures being performed per capita is on a steady incline (estimates show a rise of roughly 10% per year in both the United States and the United Kingdom), and that the lifetime attributable risk (LAR) of cancer is non-negligible for certain procedures, especially when patients receive multiple scans. One study (Brenner and Hall 2007) estimates that on the order of 2% of future cancers in the

Résumé

Dans une tomodensitométrie à la fine pointe de la technologie, l'incident de la fluence des rayons X sur le patient se limite essentiellement à une certaine forme (ou modèle) entre les projections (à l'aide d'un filtre en forme de nœud papillon, par exemple), ne permettant qu'aux biais de la fluence de se modifier (par la modulation d'un courant en forme de tube, par exemple). Permettre au modèle de fluence des rayons X de se modifier indépendamment pour chaque projection constitue un nouvel aspect de la tomodensitométrie modulée par un champ de fluence et est essentiel pour créer une qualité d'image prescrites par l'utilisateur qui répondent précisément aux besoins des patients ou des tâches à effectuer, tout en réduisant l'exposition totale du patient. Dans le présent travail, les auteurs étudient les avantages liés au bruit et à la dose quant à l'application d'une tomodensitométrie modulée par un champ de fluence (FFMCT) à certaines applications d'imagerie thoracique, dont l'examen courant du thorax, le dépistage du cancer du poumon et la tomodensitométrie cardiaque. Les modèles de fluence modulée pour un ensemble de données simulées sont créés en utilisant un script d'optimisation de recuit simulé.

La dose résultante et les distributions du rapport signal/bruit (SNR) sont comparées à celles qui sont optimisées à l'aide d'un filtre en forme de nœud papillon et de la modulation d'un courant en forme de tube. Les résultats indiquent que la FFMCT a le potentiel d'accomplir des distributions du SNR variant selon les régions en bon accord avec les valeurs prescrites par l'utilisateur et avec moins de doses totales qu'avec les techniques conventionnelles de minimisation de doses.

United States may be attributable to radiation from current CT studies.

Risks due to X-ray radiation arise because CT generates high-resolution three-dimensional (3D) images from a set of X-ray radiographs (or projections), which are recorded at different angles about a patient. Generally, noise and dose share an inverse relationship in CT: decreases in exposure (and therefore dose) are accompanied by increases in noise. The goal is then to achieve a diagnostic-quality image while limiting dose as much as possible. In practice, dose to the patient is managed by applying appropriate patient- and/or task-specific tube current and energy settings on the CT unit. The energy is typically fixed based on the patient size, while the tube current can vary throughout the scan to accommodate changes in patient thickness as a function of angle or longitudinal position—referred to as angular (Papadakis et al. 2007; Giacomuzzi et al. 1996; Greess et al. 2002; Kalender et al. 1999; Kopka et al. 1995; Lehmann et al. 1997) and z-axis tube current modulation (TCM) (Imai et al. 2009; Kalra et al. 2004; Namasivayam et al. 2006; Westerman 2002) respectively. Bowtie filters (Barrett and Swindell 1981; Graham et al. 2007; Mail et al. 2009), placed in front of the beam as shown in Figure 1, have also long been used to try to achieve more uniform exposure levels at the detector, with the benefits of decreasing dose to thinner regions of the patient while also achieving more uniform noise characteristics.

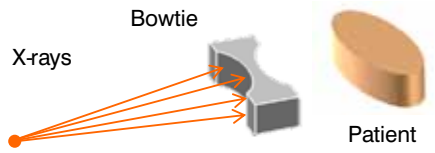

Figure 1: Schematic diagram of a bowtie attenuation filter. This filter is used to attenuate an incident X-ray beam more strongly toward the edges of a patient where the patient thickness is thinner.

More recently, innovative approaches applying more severe collimation of the beam (Chen et al. 2009; Chityala et al. 2004; Moore et al. 2006; Schafer et al. 2010; Cho et al. 2009), such that high exposure is limited to a small central region of interest, have also been proposed for large field-of-view circular CT geometries. In this case, the goal is to maintain high image quality for the target region of interest, while allowing image quality to be reduced elsewhere. These approaches have been referred to as region-of-interest imaging; however, they have not yet been adopted in practice. Dynamic collimation in the longitudinal patient direction is a recent feature that has been added to scanners to reduce radiation from the endpoints of helical scanning acquisitions, which are generally not utilized in the image reconstruction. While these techniques collectively make strides toward reduction of patient dose, the ability to manage the incident exposure is constrained to a fixed collimator or beam-

shaping filter, therefore greatly limiting the ability to compensate for the complexity of real patient anatomy in optimization of noise and dose to the patient.

Previous work (Bartolac et al. 2011; Graham 2006) has shown that allowing the fluence (number of photons per unit area) to change across the detector, both as a function of position across the detector, ξ, and as a function of angular position, θ, around the patient, may have the potential for achieving user-prescribed noise characteristics as well as significant decreases in dose. This concept, referred to as fluence-field-modulated computed tomography (FFMCT), is illustrated in Figure 2. FFMCT shares parallels with intensity-modulated radiation therapy (IMRT), except "image quality plans" replace the target "dose plans" of IMRT.

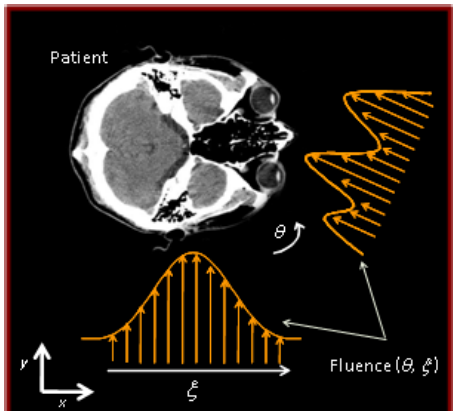

Figure 2: Schematic illustration of the method proposed for FFMCT. The pattern of incident fluence can change as a function of rotation angle about the patient as well as linear distance across the field of view.

Although FFMCT has shown potential for reducing dose while obtaining target image quality, the application considered previously (Bartolac et al. 2011) was artificial, with an arbitrarily identified region of interest. In this paper, we attempt to evaluate the dose and noise benefits of FFMCT in specific imaging applications of the thorax: lung screening, cardiac CT, and routine chest imaging. To date, delivery of modulated fluence fields in computed tomography applications remains a technical challenge. This paper, therefore, studies the potential contributions of FFMCT under simplifying assumptions in simulation.

Methods & Materials

FFMCT proceeds by optimizing the incident fluence field to deliver a prescribed image quality under dosimetric constraints. The fluence can ideally change as a function of detector position, ξ, and angular position, θ (see Figure 2). In the following study, we consider the case of a single slice acquisition of a chest CT scan, optimized for three different cases:

(1) Cardiac CT
(2) Lung Screening
(3) Routine Chest Exam

Implicit in the approach for FFMCT is that an a priori model of the patient is available. This model is used to define an image quality plan, and to predict noise and dose outcomes in order to optimize the incident fluence. In many cases, a previous CT scan of the patient may be available for this purpose. Alternatively, a population-based model could be used. In this study, a simulated anthropomorphic chest phantom, containing bony anatomy, soft-tissue, and lung-equivalent regions, was used; it is depicted in Figure 3(a).

The boundaries for the high signal-to-noise ratio (SNR) values, shown in red in Figure 3(b–d), were chosen to contain a region slightly larger than the regions of interest. The regions of interest were selected to contain the imaging target in each application (e.g., region containing the heart for cardiac CT, lung for lung screening, etc.), and are illustrated graphically in the bottom right corners of Figure 3(b-d).

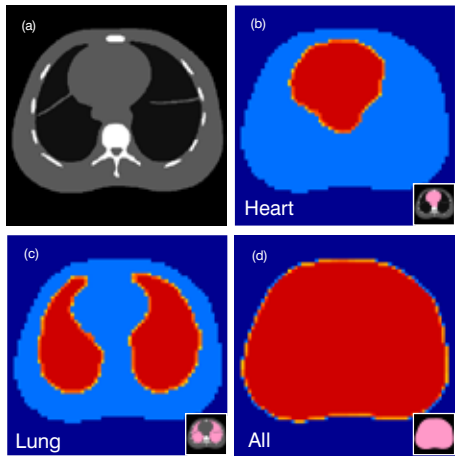

Figure 3: (a) Illustration of the simulated anthropomorphic chest phantom used in this study. Prescribed SNR distributions, where red is equivalent to a high SNR value, are shown for the cases where the scanning priority is (b) heart, (c) lung, and (d) entire patient. The region of interest delineated on image (a) is shown in the bottom right corner of images (b)–(d).

Optimization was performed considering a simplified parallel ray geometry, and considering only the primary fluence (no scattered radiation) in evaluations of dose and noise. These assumptions and their implications are discussed below in the Discussion section of this paper. The fluence arriving at the detector can then be modelled as a function of ξ and θ (with units of photon counts per detector pixel), $N(\xi,\theta)$. Optimization assumes the modulation of an arbitrary incident reference fluence field. If the reference X-ray beam is modulated by a factor of $m(\xi,\theta)$, the modulated fluence arriving at the detector can be modelled as (Bartolac et al. 2011):

$$N'(\xi,\theta) = m(\xi,\theta)N(\xi,\theta), \quad [1]$$

where the factor m is the *modulation factor*; the set of modulation factors over the complete angular and linear range will likewise be referred to as the *modulation profile*. In addition, the commonly employed filtered back-projection reconstruction algorithm was utilized in the present study. Optimization proceeds using an iterative optimization scheme that searches for the optimal modulation profile, $\hat{\mathbf{m}}$, by attempting to solve the following minimization problem:

$$\hat{\mathrm{m}} = \arg\min_{\mathrm{m}\in\mathrm{M}} \left(\sum_{\vec{r}} W_Q(\vec{r})(\dot{Q}(\vec{r}) - Q_{\mathrm{m}}(\vec{r}))^2 + \sum_{\vec{r}} W_D(\vec{r})(D_{\mathrm{m}}(\vec{r}))^2 \right) \quad [2]$$

where M is the set of all feasible modulation profiles m, $\dot{Q}(\vec{r})$ is the desired or prescribed quality metric at spatial position $\vec{r} = (x, y, z)$, $Q_{\mathbf{m}}(\vec{r})$ is the modulation-dependent, spatially variant quantification of the image quality within the object, $D_{\mathbf{m}}(\vec{r})$ is the local, modulation-dependent dose, and $W_Q(\vec{r})$ and $W_D(\vec{r})$ are predefined, spatially varying weighting factors that can be used to prioritize image quality and dose, respectively, at specific regions.

In the present study, the metric for image quality, $Q(\vec{r})$, was defined as the standard deviation of the reconstructed signal, $n(\vec{r})$, relative to a reference value for the attenuation coefficient of water, μ_{H_2O}:

$$Q(\vec{r}) = \frac{\mu_{H_2O}}{n(\vec{r})} \quad [3]$$

A higher Q value indicates better image quality (lower noise) and can easily be interpreted as equivalent to a high SNR with respect to water. That being said, since the noise is considered relative to a constant reference signal, it should be noted that this measure of quality is strictly a measure of the noise and is independent of the mean values in the reconstruction volume. However, since the units are the same as SNR and can be interpreted similarly, it will be useful to refer to the quality metric Q as SNR for simplicity here. Note that other quality metrics could also have been used, such as contrast-to-noise ratio (CNR).

The first term in equation causes the solution to trend toward the prescribed SNR criteria, while the second term attempts to lower the dose as much as possible. The weights can be altered to change the priority of the SNR or dosimetric terms. A logical choice of dosimetric weights might be the organ-specific weights provided by the International Commission on Radiological Protection (ICRP). In that case, the second term would attempt to minimize the effective dose. In this study, the dosimetric weighting was set to unity for all voxels, such that each voxel has equivalent priority in the optimization scheme with respect to dose minimization. A higher weighting (by a factor of 10) was applied to the prescribed high-quality region of interest for the SNR term in order to prioritize image quality in these regions. Computation of equation at each iteration required a prediction of the standard deviation as a function of voxel position. For this purpose we used a model for the variance of the noise, derived by Kak and Slaney (1988) for the case of parallel-ray, filtered back-projection reconstruction methods:

$$\mathrm{var}\left(f(\vec{r})\right) = \left(\frac{\pi\tau}{M_{proj}}\right)^2 \sum_{\theta}\sum_{\xi}\frac{1}{N'(\theta,\xi)}h^2(x\cos\theta + y\sin\theta - \xi) \quad [4]$$

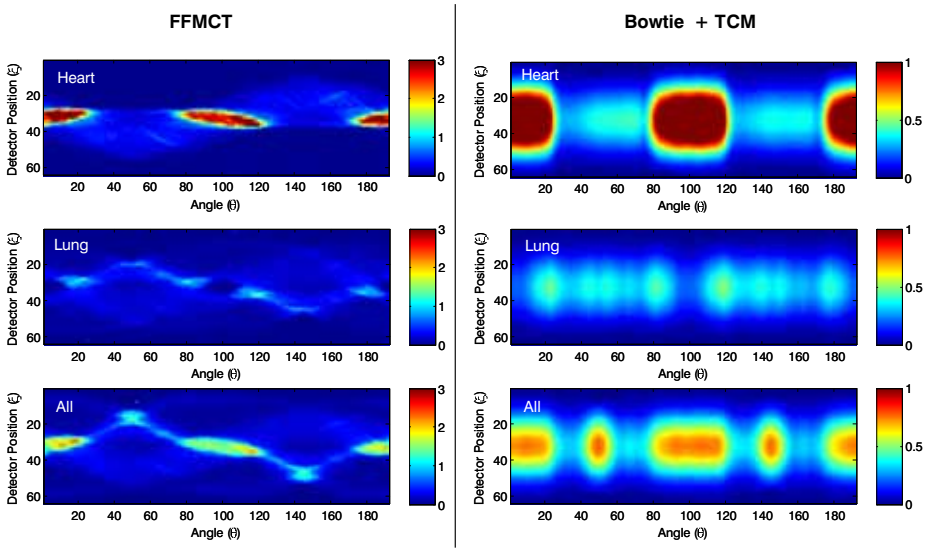

Figure 4: Modulation profiles showing the optimized modulation factors as a function of linear direction across the field of view, and the projection angle. Each column in a given modulation profile dictates the modulation applied to the fluence for a particular projection. FFMCT results show increased complexity compared with the bowtie filter results.

where *Mproj* is the number of projections, *t* is the width of the detector pixels, and *h* is the convolution kernel in the filtered back-projection operation. Simulations verified that this expression was accurate to within 5% for the prediction of the variance (or standard deviation squared). Optimization of equation was carried out using a simulated annealing optimization method, described in detail in a previous publication (Bartolac et al. 2011). Dose calculations were modelled from the collision kerma, $K_c(\vec{r})$, which accurately represents the dose at energy levels used in computed tomography:

$$D(\vec{r}) \simeq K_c(\vec{r}) = \Psi(\vec{r})\frac{\mu_{en}(\vec{r})}{\rho(\vec{r})} \quad [5]$$

where $\Psi(\vec{r})$ is the primary energy fluence, assuming each photon has an energy of 60 keV, $\mu_{en}(\vec{r})$ is the mass-energy absorption coefficient, and $\rho(\vec{r})$ is the material density. In order to reduce the computation time required for the optimization, low-resolution images were considered of the input model and for the target image quality plans (64×64 bins, 0.54×0.54×0.54 cm voxel size). For comparison of the results, the optimization was repeated by constraining the modulation profile for each projection to the shape of a bowtie filter. This situation can be viewed as equivalent to applying tube current modulation with a bowtie filter in place, except the degree of bias applied in tube current modulation is optimized using the methods defined above. In this way, the bowtie plus tube current modulation can be viewed as FFMCT applied using a constrained modulator. Dose outcomes were compared considering integral dose (in joules) as well as the relative distribution of dose achieved in each situation.

Finally, sample reconstructions of images that included Poisson noise based on the prescribed modulation profiles are shown in order to visualize the impact of fluence modulation in practice.

Results

Figure 4 shows the resulting modulation profiles for each of the three thorax CT imaging cases identified. The larger number of degrees of freedom in FFMCT resulted in more complex fluence patterns for each of the cases when compared with the patterns produced using the bowtie filter. However, it can be observed that the modulation profiles constrained to the bowtie filter show peaks in tube current at similar projection intervals to those of the FFMCT cases.

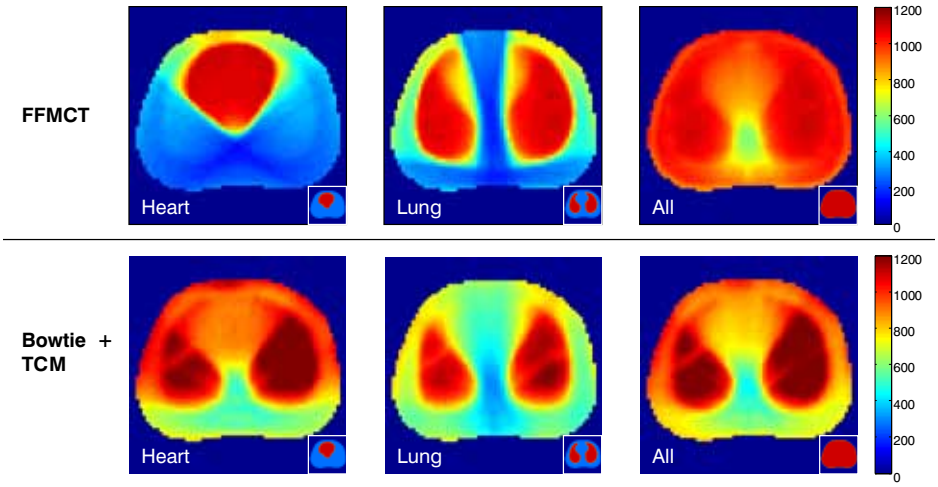

Figure 5: Predicted SNR distributions resulting from the modulation profiles shown in Figure 4. The bottom right corner of each image shows the prescribed SNR distribution. FFMCT resulted in better agreement with the prescribed values than the bowtie filter with tube current modulation.

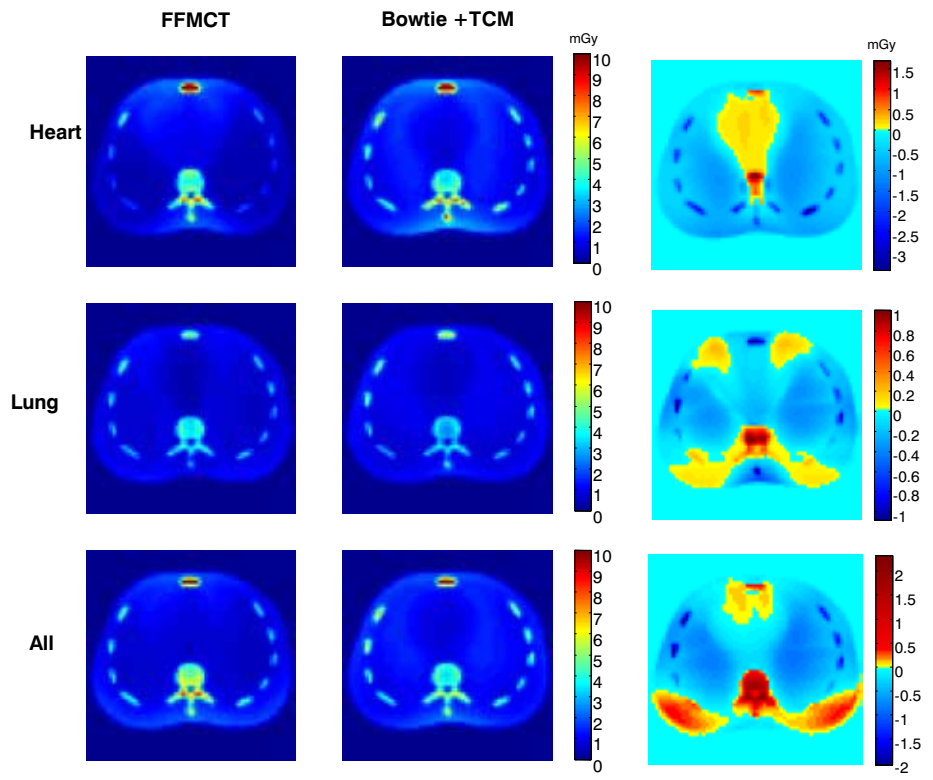

Figure 6: Dose distributions for different thoracic imaging cases when using FFMCT as compared to a bowtie filter with tube current modulation. The difference images on the right highlight regions of relative increases and decreases in dose of FFMCT with respect to the distributions arising from the bowtie filter with tube current modulation.

Predicted SNR outcomes for the FFMCT and bowtie cases are compared in Figure 5. FFMCT resulted in SNR distributions with greater similarity to the prescribed values for all three cases than use of the bowtie filter. In contrast, the SNR distributions arising from the bowtie filter showed little change in overall pattern, with the region of highest image quality consistently trending within the region of the lungs for each of the imaging cases presented. Higher uniformity over the prioritized high-SNR regions was also observed for the FFMCT cases, compared with results for use of the bowtie filter with tube current modulation.

Figure 6 shows dose comparisons for the three scenarios under the differing constraints. Integral dose decreases (in joules) were found to be 23% for the heart, 5% for the lung, and 4% for the routine diagnostic cases when compared with use of the bowtie filters. Figure 6 also shows the subtraction images of the dose distributions, indicating that both relative increases and decreases in dose occurred for the FFMCT cases, compared with use of the bowtie filter with tube current modulation (warm colours indicate increases).

High-resolution image reconstructions with added simulated noise predicted by the FFMCT modulation profiles for the routine diagnostic and lung screening exams are shown in Figure 7, for comparison with the predicted SNR outcomes. Figure 7(b) shows that greater noise and corresponding streak artifacts are evident in the lung screening case but do not impede visualization of the lesion within the region of interest within the lungs, where image quality remains consistent with that of the routine diagnostic scan. An added soft-tissue lesion with a deviation of approximately 4% in signal value is also seen in Figure 7(c), shown at a different contrast level and corresponding to the boxed region in Figure 7(b).

Discussion

This study was carried out to evaluate whether potential noise and dose benefits exist when applying FFMCT to specific imaging tasks of the thoracic region. The results indicated that FFMCT could potentially meet user-prescribed image quality criteria to a higher degree over what could be achieved by conventional modulator designs in practice today. Benefits were particularly pronounced for the case of cardiac CT, where FFMCT achieved approximately 23% integral dose reduction and higher, more uniform SNR values within the region of interest. While FFMCT application to the routine chest

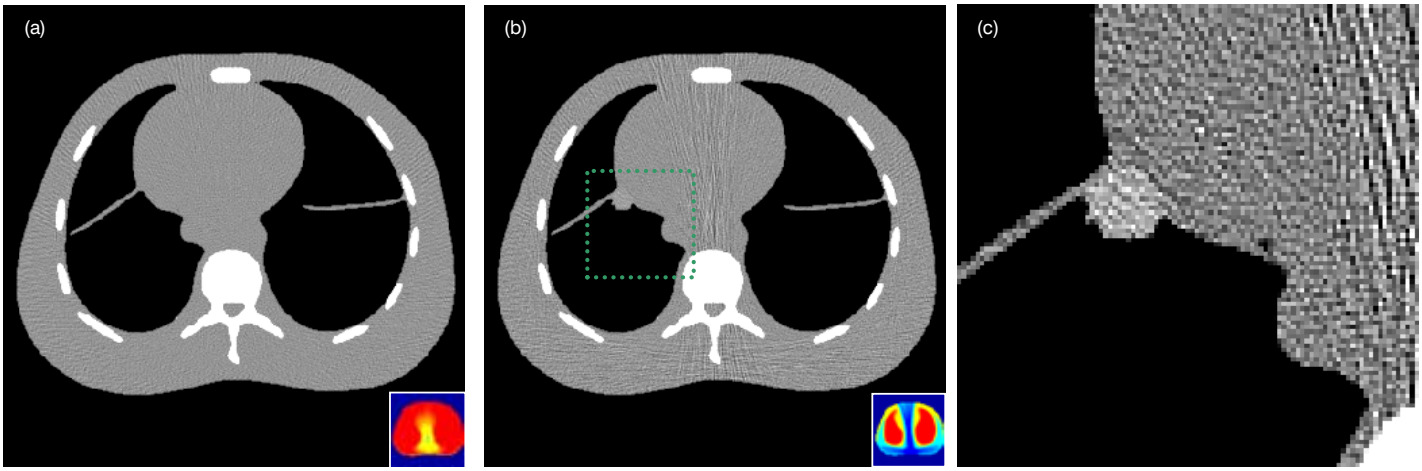

Figure 7: Reconstructed images with added Poisson noise for (a) routine chest exam and (b) lung screening test. (c) A close-up of the boxed region in (b) shows a simulated lesion with a 4% signal deviation from soft tissue, observable within the lung due to the higher SNR value within the lung. Predicted SNR distributions for (a) and (b) are shown in the bottom right corners for comparison. Streaks and noise in (b) closely follow the predicted regions of reduced image quality (blue regions).

exam achieved more modest reduction in integral dose, the SNR distribution was much more uniform, suggesting greater utility in the scan without added dose response. Similarly, high SNR values were also more uniform and consistent with the prescribed target values over the entire region of interest for the FFMCT lung screening case. Interestingly, though, the anatomic variations in the simulated phantom seemed to produce an inherent result of lower noise in much of the region of the lungs, as suggested from the different bowtie filter cases; this can be understood by considering that the attenuation is weakest through the region of the lungs, so a larger number of photons reach the detector in this case for most angles. We note that while the bowtie filter was included for comparative purposes, the manner in which the tube current modulation was optimized in itself can be viewed as an application of FFMCT, except where the modulation is placed under additional constraints (in this case, the shape of the bowtie filter). In this way, an interesting result of this study was the application of FFMCT in optimizing modulation profiles for existing compensators and tube current controls that are currently used.

One limitation of the study was the absence of scatter contribution from within the body as well as potentially from the modulator itself. Work remains to study the implications of scatter on image quality and dose contribution, which may be quite large. However, previous work suggests that image quality may be improved by scatter reduction within the high-SNR regions of interest; similarly, reductions in primary fluence suggest reductions in dose due to scatter as well.

While the technical challenge for delivering such modulated fluence fields has not been resolved, at least one application, using an "electronic bowtie" arrangement composed of multiple sources in an inverse CT geometry, has shown the potential for fluence modulation delivery in real applications, even under broad constraints. Furthermore, fluence delivery methods of IMRT could potentially be adopted in CT.

Conclusions

The results of this study support the hypothesis that FFMCT can potentially be employed to decrease dose to the patient while achieving image quality to a level prescribed by the user. Specifically, three specific thoracic imaging tasks were considered that showed that FFMCT could potentially reduce dose and significantly improve image quality in the related regions of interest when compared with conventional dose reduction methods.

References

Barrett HH, Swindell W. (1981). Radiological imaging: The theory of image formation, detection, and processing. New York: Academic Press.

Bartolac S, Graham SS, Siewerdsen J, Jaffray D. (2011). Fluence field optimization for noise and dose objectives in CT. Med Phys 38 Suppl 1, S2.

Brenner DJ, Hall EJ. (2007). Computed tomography—an increasing source of radiation exposure. N Engl J Med 357, 2277-2284.

Chen L, Shen Y, Lai CJ, Han T, Zhong Y, Ge S, Liu X, Wang T, Yang WT, Whitman GJ, Shaw CC. (2009). Dual resolution cone beam breast CT: A feasibility study. Med Phys 36, 4007-4014.

Chityala RN, Hoffmann KR, Bednarek DR, Rudin S. (2004). Region of interest (ROI) computed tomography. Proc. SPIE 5368, 534-541.

Cho S, Pearson E, Pelizzari CA, Pan X. (2009). Region-of-interest image reconstruction with intensity weighting in circular cone-beam CT for image-guided radiation therapy. Med Phys 36, 1184-1192.

De Man B, Basu S, Fitzgerald P, Harrison D, Iatrou M, Khare K, LeBlanc J, Senzig B, Wilson C, Zhye Y, & Pelc N. (2007). Inverse geometry CT: The next-generation CT architecture?," Nuclear Science Symposium. Conference Record, NSS '07. IEEE 4, 2715–2716.

Giacomuzzi SM, Erckert B, Schopf T, Freund MC, Springer P, Dessl A, Jaschke W. (1996). The smart-scan procedure of spiral computed tomography: A new method for dose reduction. Rofo 165, 10-16.

Graham SA. (2006). Intensity Modulated Cone-Beam CT [MSc thesis]. Toronto: University of Toronto.

Graham SA, Moseley DJ, Siewerdsen JH, Jaffray DA. (2007).Compensators for dose and scatter management in cone-beam computed tomography. Med Phys 34, 2691-2703.

Greess H, Nomayr A, Wolf H, Baum U, Lell M, Bowing B, Kalender W, Bautz WA. (2002). Dose reduction in CT examination of children by an attenuation-based on-line modulation of tube current (CARE Dose). Eur Radiol 12, 1571-1576.

Guthrie C. (2008). How Dangerous Are CT Scans? Time Magazine [Internet]. [cited 2012, July 18]; (Friday, June 27, 2008). Available from: http://www.time.com/time/health/article/0,8599,1818520,00.html

Hillman BJ, Goldsmith JC. (2010). The uncritical use of high-tech medical imaging. N Engl J Med 363, 4-6.

Imai K, Ikeda M, Enchi Y, Niimi T. (2009). Quantitative assessment of image noise and streak artifact on CT image: Comparison of z-axis automatic tube current modulation technique with fixed tube current technique. Comput Med Imaging Graph 33, 353-358.

Kak AC, Slaney M. (1988). Principles of computerized tomographic imaging. New York: IEEE Press.

Kalender WA, Wolf H, Suess C, Gies M, Greess H, Bautz WA. (1999). Dose reduction in CT by on-line tube current control: Principles and validation on phantoms and cadavers. Eur Radiol 9, 323-328.

Kalra MM, Maher MM, Toth TL, Kamath RS, Halpern EF, Saini S. (2004). Comparison of Z-axis automatic tube current modulation technique with fixed tube current CT scanning of abdomen and pelvis. Radiology 232, 347-353.

Kopka L, Funke M, Breiter N, Hermann KP, Vosshenrich R, Grabbe E. (1995). An anatomically adapted variation of the tube current in CT: Studies on radiation dosage reduction and image quality. Rofo 163, 383-387.

Lehmann KJ, Wild J, Georgi M. (1997). Clinical use of software-controlled x-ray tube modulation with "Smart-Scan" in spiral CT. Aktuelle Radiol 7, 156-158.

Mail N, Moseley DJ, Siewerdsen JH, Jaffray DA. (2009). The influence of bowtie filtration on cone-beam CT image quality. Med Phys 36, 22-32.

Moore CJ, Marchant TE, Amer AM. (2006). Cone beam CT with zonal filters for simultaneous dose reduction, improved target contrast and automated set-up in radiotherapy. Phys Med Biol 51, 2191-2204.

Namasivayam S, Kalra MK, Pottala KM, Waldrop SM, Hudgins PA. (2006). Optimization of Z-axis automatic exposure control for multidetector row CT evaluation of neck and comparison with fixed tube current technique for image quality and radiation dose. AJNR Am J Neuroradiol 27, 2221-2225.

Papadakis AE, Perisinakis K, Damilakis J. (2007). Angular on-line tube current modulation in multidetector CT examinations of children and adults: The influence of different scanning parameters on dose reduction. Med Phys 34, 2864-2874.

Schafer S, Noel PB, Walczak AM, Hoffmann KR. (2010). Filtered region of interest cone-beam rotational angiography. Med Phys 37, 694-703.

Smith-Bindman R. (2010). Is computed tomography safe? N Engl J Med 363, 1-4.

Westerman BR. (2002). Radiation dose from Toshiba CT scanners. Pediatr Radiol 32, 735-737; discussion 751-754.